*Science on Form: Proceedings of the Second International Symposium for Science on Form*,
Editor: S. Ishizaka, pp. 157–174.


# QUASI-STATIC SIMULATION OF LIQUEFACTION PHENOMENA IN GRANULAR MATERIALS

Yuji KISHINO

*Department of Civil Engineering, Tohoku University, Aoba, Sendai 980, Japan*

key words: Granular materials, Simulation, Liquefaction, Dissipation energy

**Abstract.** To investigate the liquefaction phenomena from the microscopical point of view, the undrained cyclic test on granular materials was simulated by the use of a new computational method called the granular element method. The test results of macroscopic quantities were qualitatively similar to the results obtained by usual tests on real sands. The detailed investigation on the dissipation mechanism gave a new insight into the deformation characteristics of granular materials. For example, it was found that the number of contact points which share the dissipation energy in each loading step is limited and that there exists a tendency that the distribution of dissipation energy is inhomogeneous when the large pore water pressure arises.

## INTRODUCTION

Recently, the granular materials has been studied from the micromechanical aspects (Satake and Jenkins: 1988). In such approaches, microscopical observations of the mechanical behaviors of granular systems are required. However, it is hard to achieve this in actual experiments on sands, gravels or other real granular materials. On the other hand, experiments on granular models can offer various kinds of micromechanical informations. As one of the possibilities, the photoelasticity tests on two dimensional models may be used (Drescher and de Josselin de Jong: 1972). However, the photoelasticity tests alone are insufficient for the detailed discussion, even though some kinds of micromechanical quantities are obtained through elaborative processes. Another approach is the numerical experiments in computers, which may be the most powerful procedure to study the micromechanics.

As a computer simulated method for granular materials, the distinct element method has been developed (Cundall and Strack: 1979). The procedure of the analysis adopted in the distinct element method is based on the finite difference scheme for solving the Newton's equation, and the basic equations are uncoupled simultaneous equations. As the stiffness matrix is not taken into account in the final

This paper was presented at The Second International Symposium for Science on Form (October 19th–21st, 1988 at the University of Tsukuba, Japan).

equations, the special care should be paid when it is applied to the quasi-static analyses of dense granular assemblies.

The author developed a new simulation method to analyze the quasi-static problems of granular materials (Kishino: 1988). The algorithm of this method is given in the following section. In the latter half of this paper, the result of a numerical simulation of cyclic undrained test is shown and the dissipation mechanism in liquefaction phenomena is discussed.

## GRANULAR ELEMENT METHOD

The new method presented here is developed mainly for the precise investigation of quasi-static behavior of granular materials and it is called the granular element method. In this section the outline of this method is explained.

*Basic idea of the granular element method*

The granular element method used in this paper is based on the following basic idea:

a) The numerical model of granular material consists of two types of element. One is called the granular element which is placed at the inner part of the region. The other one is called the boundary element which is located along the peripheral part of the region. The boundary element transmits the external force to the granular elements.

b) The elements in the model are assumed to be rigid. However, they can overlap each other. Usually, the amount of overlapping is small enough compared with the dimensions of granular elements, so that the deformation of granular assembly is mainly governed by the rearrangement of granular elements.

c) Only when two elements overlap, a contact force is generated between them. The amount of contact force depends on springs attached virtually at contact point. The virtual springs represent the elasticity of grains.

d) For the slippage between elements, the Coulomb's friction law is assumed, and the tangential component of contact force can not exceed the limit determined by this law.

e) To get the equilibrium state, each element is iteratively translated and rotated according to the contact stiffness matrix determined with respect to the relative locations of neighboring elements.

The employment of rigid elements and virtual springs is the same idea as in the distinct element method. However, this method uses the stiffness matrices strictly in the determination of incremental movements of grains, while the distinct element method is based on the forward difference approximation of the Newton's second law. When grains are packed densely and change their locations quasi-statically, it is quite natural to use a stiffness method to determine the movements of grains. The directions of incremental movements determined by both methods do not generally coincide when a grain moves under the constraint from neighboring elements. Further, the granular element method requires no damping factors for the stable conversion to the solution.

The flow chart of the granular element method is given in Fig. 1. As shown in

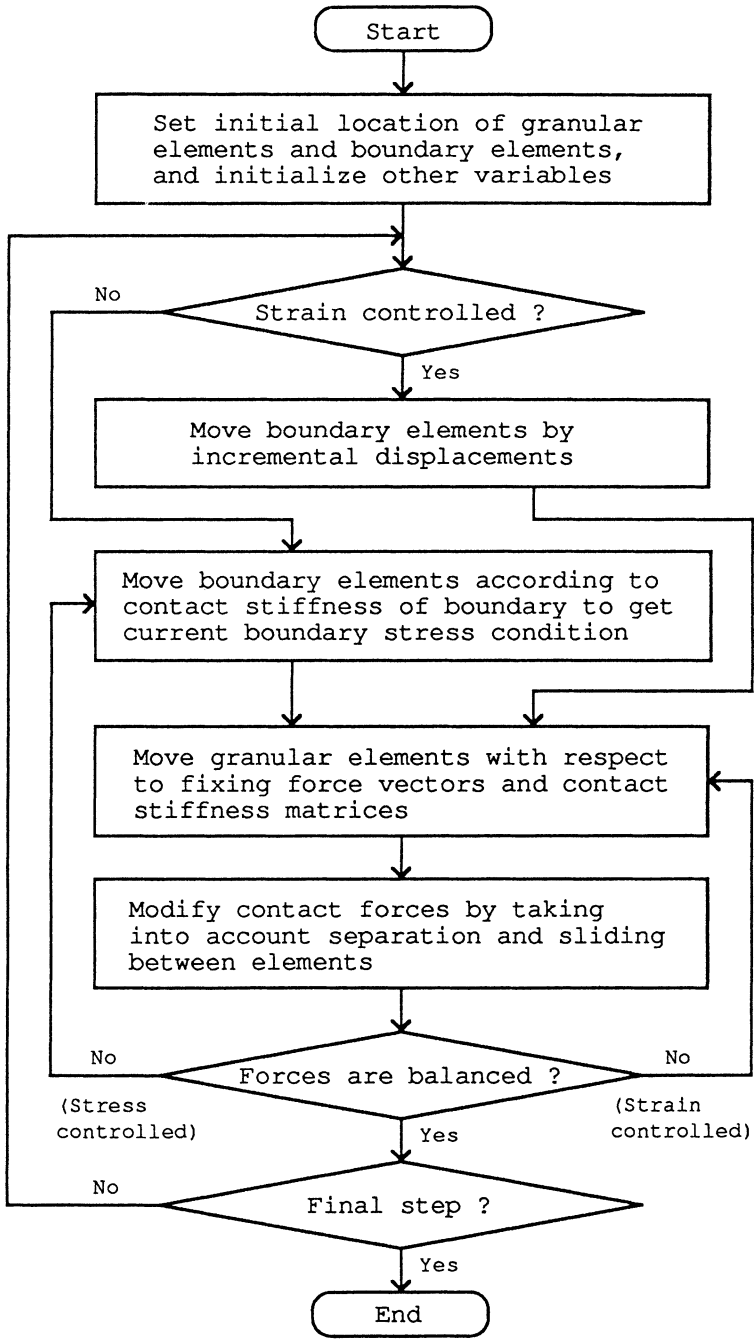


Fig. 1. Flow chart of the granular element method.

the flow chart, the granular element method adopts an iterative procedure. This is because the iterative procedure simplifies the algorithm of calculation by computers. The choice of routines in the iterative procedure depends on the boundary condition as shown in the flow chart. The initial arrangement of granular elements within the region surrounded by boundary elements can be obtained by applying the granular element method itself to an original packing. Even if the original packing is artificial and the equilibrium condition is not fullfilled, the equilibrated state can be attained through the iterative process.

The detailed explanation which can be applied strictly to the two dimensional problems is given in the following subsections.

*Force-displacement law between elements*

In Fig. 2, $A$ and $B$ are the typical granular elements in a two-dimensional granular assembly and they are in contact with each other at contact point $C$. The contact force $\boldsymbol{p}$ acting on grain $A$ has the normal and tangential components; $p_n \equiv -\boldsymbol{p}\cdot\boldsymbol{n}$ and $p_t \equiv -\boldsymbol{p}\cdot\boldsymbol{t}$. To introduce the formulation with matrices, the contact force is expressed in a vectorial form; $P_C \equiv (p_n, p_t)_C^t$.

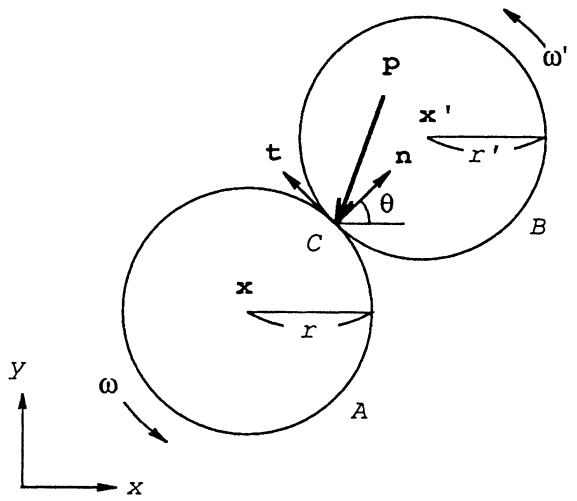


Fig. 2. Contact force between granular elements.

The incremental movement of grain $A$ with radius $r$ consists of the translation $\Delta \boldsymbol{x}$ and the rotation $\Delta\omega$, and it is denoted in a vectorial form; $\Delta X \equiv (\Delta x, \Delta y, r\Delta\omega)^t$. By this movement of grain $A$, the following relative displacement is induced between grains $A$ and $B$:

$$\Delta U_C \equiv (\Delta u_n, \Delta u_t)_C^t = T_C \Delta X \tag{1}$$

where

$$T_C \equiv \begin{bmatrix} \cos\theta & \sin\theta & 0 \\ -\sin\theta & \cos\theta & 1 \end{bmatrix}_C \tag{2}$$

is a transformation matrix and $\theta$ is the direction angle of $\boldsymbol{n}$ measured from $x$ axis as shown in Fig. 2.

The relationship between contact force and relative displacement is assumed to be represented by a couple of linear springs in the normal and tangential directions with the spring constants $k_n$ and $k_t$. Then, the incremental relationship between contact force and relative displacement is given by the following equation:

$$\Delta P_C = S_C \Delta U_C \tag{3}$$

where

$$S_C \equiv \begin{bmatrix} k_n & 0 \\ 0 & k_t \end{bmatrix}_C \tag{4}$$

is the stiffness at the contact point $C$.

When either of the neighboring elements is a boundary element, the stiffness at this contact point is also defined in the same manner. These linear relationship between contact force and relative displacement is inevitably lost when the separation or sliding takes place between elements. As explained later, the non-linearity in force-displacement relation is taken into account by modifying the contact forces obtained through Eq. 3.

*Fixing force vector*

In the granular element method, an iterative process is adopted to get the equilibrated state of contact forces $\boldsymbol{p}$ and body forces $\boldsymbol{b}$ for all granular elements. Thus, while the iterative calculation is proceeding, the resultant force applied to a granular element may not equal zero unless the additional force $\boldsymbol{f}$ and moment $m$ are virtually applied at the center of granular element as shown in Fig. 3. The virtual

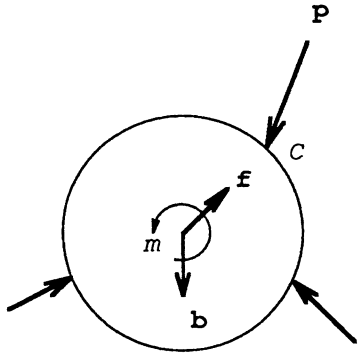


Fig. 3. Fixing force and moment.

force and moment which are required to fix each granular element in the inequilibrated state, form the fixing force vector; $F \equiv \left(f_x, f_y, \frac{m}{r}\right)^t$. By the definition of fixing force vector, $F$ is equated as follows:

$$F = \Sigma_C \, T_C^t P_C - B \tag{5}$$

where $B \equiv (b_x, b_y, 0)^t$ is the body force vector, and $\Sigma_C$ stands for the summation over the contact points on a granular element.

*Contact stiffness matrix*

The contact stiffness matrix gives the incremental force and moment generated by the unit movement of a granular element whose neighboring elements are assumed to be fixed, and it is derived in the following manner.

When a granular element with contact point $C$ is subjected to the incremental movement $\Delta X$, the increment of contact force at $C$ is obtained through Eq. 1 and Eq. 3 as

$$\Delta P_C = S_C T_C \Delta X. \tag{6}$$

Thus the increment of fixing force vector induced by $\Delta X$ is derived through Eq. 5 and Eq. 6 as the following equation:

$$\Delta F = S \Delta X \tag{7}$$

where $S \equiv \Sigma_C T_C^t S_C T_C$ is the contact stiffness matrix. The contact stiffness matrix of a granular element is determined with respect to the relative locations of the neighboring elements and it is revised step by step in the process of iteration.

If only one granular element is allowed to move while the other elements being fixed, then the fixing force vector can be released by the following equation:

$$F + \Delta F = 0. \tag{8}$$

Thus, for the case that $\det S \neq 0$, the incremental movement of the granular element is determined by the following equation:

$$\Delta X = - S^{-1} F. \tag{9}$$

In the next section, Eq. 9 is modified to take into account the simultaneous movements of the neighboring granular elements.

*Releasing of fixing force vector*

As shown in Fig. 1, the equilibrium state of granular assembly at each loading step is attained by releasing the fixing force vectors iteratively. The iterative process has been adopted because it simplifies the algorithm of calculation, in which the contact stiffness matrix $S$ changes successively according to the rearrangement of

granular elements and its determinant sometimes becomes zero.

If the releasing of fixing force vector with Eq. 9 is executed for only one granular element in one calculation step, the order of releasing affects the results of analysis. This is because the releasing of a fixing force vector affects the successive determination of other fixing force vectors. To avoid this, all fixing force vectors, as well as all contact stiffness matrices, are calculated at the same time with respect to the last locations of granular elements. Then, the fixing force vectors for all the granular elements are simultaneously revised toward the complete releasing.

As the determinant of the contact stiffness matrix $S$ can be equal to zero, Eq. 9 should be modified according to the type of singularity as explained in the following:

a) In the case of $\det S \neq 0$, the movement of granular element is determined by the equation

$$\Delta X = -\alpha S^{-1} F \tag{10}$$

where $\alpha$ is the modification factor. As the neighboring granular elements are moved at the same time, the amount of $\alpha$ should be less than 1.

b) In the case of $\det S = 0$ with no contact point, the movement of the granular element should follow the motion governed by the Newton's second law. However, in the quasi-static problems as dealt in this paper, the dynamical effects may be neglected. Thus, the granular element is translated gradually in the direction of body force. As the amount of the translation should be comparable with the movements of the other granular elements in the region, the incremental movement is given by

$$\Delta X = \frac{\beta}{k_n} B \tag{11}$$

where the amount of the factor $\beta$ is usually greater than 1.

c) In the case of $\det S = 0$ with only one contact point, the translation in the direction of contact normal is determined as in the case a). On the other hand, the movement in the tangential direction is determined as in the case b) with the assumption that the tangential component of relative displacement is zero; $\Delta u_t = 0$. Thus, the incremental movement is given by the following equation:

$$\Delta X = \frac{1}{K_n} \begin{bmatrix} \cos\theta & -\sin\theta \\ \sin\theta & \cos\theta \\ 0 & -1 \end{bmatrix}_C \begin{bmatrix} -\alpha' \boldsymbol{f} \cdot \boldsymbol{n} \\ \beta' \boldsymbol{b} \cdot \boldsymbol{t} \end{bmatrix}_C \tag{12}$$

where $\alpha'$ and $\beta'$ are the similar constants to $\alpha$ and $\beta$. In this case, if the tangential component of contact force at the contact point is not zero, it is set to zero to allow the free rotational movement.

d) The case of $\det S = 0$ with two or more contact points is limited to the special case that the tangential stiffnesses at contact points are zero; $k_t = 0$. In this case, by assuming that $\Delta\omega = 0$, the incremental movement of the granular element is

determined as

$$\Delta X' = -\alpha S^{-1} F' \tag{13}$$

where the primed quantities denote the quantities without rotational components.

The incremental contact forces are calculated by substituting $\Delta X$ into Eq. 6. The contact force obtained in this way should be modified if it is necessary. If the tangential component $p_n$ becomes less than zero, then the value of zero is substituted into $p_n$ as well as $p_t$. Further, when the tangential component $p_t$ exceeds the limit determined by Coulomb's law, the absolute value of $p_t$ is modified as

$$|p_t| = p_n \tan\phi + c \tag{14}$$

where $\phi$ is the friction angle and $c$ is the cohesion.

The iterative calculation is repeated until all the fixing force vectors of granular elements fulfill the condition expressed by the following equation:

$$F^t F \leq a^2 \tag{15}$$

where $a$ is the accuracy having the dimension of the force.

*Boundary element*

The boundary of granular assembly consists of a set of boundary elements. For conventional simulations of two dimensional tests, four straight walls may be used as boundary elements. For the more precise control, boundary elements can be the elements with the shapes of granular elements as shown in Fig. 4. In any case, the fixing force vector of boundary element is not equal to zero, but it is equal to the external force. The contact stiffness matrix of boundary is determined on the basis of the stiffnesses between boundary elements and neighboring granular elements.

In the following, the procedure for boundary control in the element tests (tests on specimens to get stress-strain relations) is explained. Usual tensor notation in a

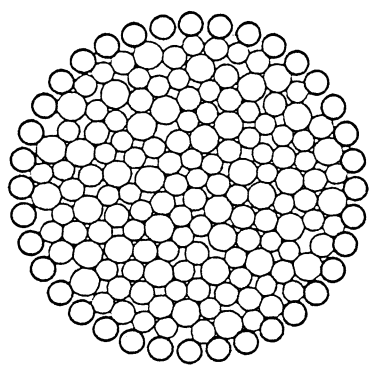

Fig. 4. Example of boundary elements.

Cartesian coordinate system is adopted for the explanation. In the element tests, the movements of boundary elements may be regulated through the linear transformation as

$$\Delta x_i = \Delta T_{ij} x_j \tag{16}$$

where $x_i$ and $T_{ij}$ ($i, j=1, 2$ for two dimensional case) are the coordinates of a point on boundary element and the transformation tensor respectively, and $\Delta$ attached to these quantities denotes the increment. For the symmetric part of the increment of transformation tensor, the following equation holds:

$$\Delta T_{(ij)} = \Delta \varepsilon_{ij} \tag{17}$$

where $\varepsilon_{ij}$ is the strain tensor and the parentheses attached to the indices on the left hand side denotes the mixing.

The stress tensor $\sigma_{ij}$ is defined on the basis of external work such that the following equation is fulfilled:

$$\Delta W \equiv \frac{1}{A} \Sigma_B f_i \Delta x_i = \sigma_{ij} \Delta \varepsilon_{ij} \tag{18}$$

where $A$ is the area of the region and $\Sigma_B$ denotes the summation over the boundary elements to which the external forces $f_i$ are applied at the points $x_i$. From the above three equations, the stress tensor is defined in terms of contact forces as

$$\sigma_{ij} = \frac{1}{A} \Sigma_B f_{(i} x_{j)} \tag{19}$$

where the following equilibrium of moment is taken into account:

$$\Sigma_B f_i x_j = \Sigma_B f_j x_i. \tag{20}$$

When the boundary movement is controlled by the strain or the displacement, the location of boundary element, which is determined at the beginning of each loading step, is maintained until the granular assembly reaches its equilibrium state. When the equilibrium state is attained, the external force applied to each boundary element is obtained by calculating the fixing force vector of the respective boundary element.

When the boundary movement is controlled by the stress, the fixing force vector of boundary element is prescribed for each loading step. The difference between the current fixing force vector and the prescribed one is eliminated by moving the boundary element according to the contact stiffness matrix of boundary. The releasing of the fixing force vectors of granular elements causes the changes in the fixing force vectors of boundary elements, so that the above procedure is repeated until the granular assembly reaches its equilibrium state.

Usually, these two types of control are mixed. For example, the conditions

controlled purely by stress should be excluded, because the rigid translation and the rigid rotation are not determined with the pure stress condition only. On the other hand, the dilatancy characteristics, which plays a central roll in the mechanics of granular materials, can not be obtained by the conditions controlled purely by strain. To derive the dilatancy characteristics, boundaries should be controlled by the mean stress instead of the volumetric strain.

The strain-controlled shearing test under constant mean pressure is an example of the mixed type of boundary condition. In this case, the incremental shearing strain is applied to the boundary elements at the beginning of each loading step, and the difference between the prescribed and current mean pressures is diminished in the way of stress-controlled procedure in which the boundary elements are controlled so as not to generate the shearing strain. After the equilibrium state for the granular assembly is obtained, further incremental shearing strain is applied to proceed to the next loading step.

Another example of the mixed type of boundary condition is the stress-controlled shearing test under constant volume. In this case the movements of boundary elements are determined by the shearing components in stress tensor and contact stiffness of boundary. The undrained condition is similar to the constant volume condition. However, the volume of the region is allowed to change slightly according to the bulk modulus of water and the isotopic component of the external stress is shared by the granular elements and the pore water. If the time effect of seepage can be omitted, the volume change induces the pore pressure immediately. The effective stress is calculated by subtracting the pore pressure from the total external stress.

The extent of the movement of boundary element at each loading step should be restricted to avoid the excessive overlapping between elements and to secure the smooth transition of the arrangement of granular elements.

*Dissipation energy*

From the simulated data on locations of elements and contact force vectors at sequential loading steps, the dissipation energy and the external work can be calculated easily as follows:

When two granular elements in Fig. 2 are subjected to the incremental translations $\Delta \boldsymbol{x}$ and $\Delta \boldsymbol{x}'$ and the incremental rotations $\Delta\omega$ and $\Delta\omega'$, then the tangential component of incremental relative displacement at contact point $C$ is expressed as

$$\Delta u_t = (\Delta \boldsymbol{x} - \Delta \boldsymbol{x}') \cdot \boldsymbol{t} + r\Delta\omega + r'\Delta\omega'. \tag{21}$$

If the tangential component of contact force changes its value by $\Delta p_t$, the elastic part of incremental relative displacement is defined as

$$\Delta u_e = \frac{1}{k_t} \Delta p_t. \tag{22}$$

Then, by putting inelastic part as

$$\Delta u_d = \Delta u_t - \Delta u_e \tag{23}$$

the incremental dissipation energy at contact point $C$ is calculated as

$$\Delta d_C = p_t \Delta u_d \tag{24}$$

where $p_t$ is the average of values for the states before and after the respective step. The above equation is valid as far as the mechanical change in granular assembly is slow.

Adding the dissipation energies at all contact points in the whole area $A$, the dissipation energy density is obtained as

$$\Delta D = \frac{1}{A} \Sigma_C \Delta d_C \tag{25}$$

where $\Sigma_C$ stands for the summation over all contact points in granular assembly.

On the other hand, the increment of external work per unit area induced by the incremental displacement vectors $\Delta \boldsymbol{x}$ of boundary elements is calculated by

$$\Delta W = \frac{1}{A} \Sigma_B \boldsymbol{f} \cdot \Delta \boldsymbol{x} \tag{26}$$

where $\Sigma_B$ stands for the summation over the boundary elements and the fixing force vector $\boldsymbol{f}$ is identical to the external force as stated in the section of *Boundary element*. The densities of total external work and dissipation energy at a certain state can be obtained by summing up all the incremental quantities in the preceding steps.

## SIMULATION OF UNDRAINED CYCLIC TEST

A simulation of undrained cyclic shearing test was performed on a two dimensional model shown in Fig. 5. The model consists of three types of discs with different diameters and each of them has the same total area. The pore was assumed to be filled with water and the zero pore pressure was assumed in the initial state. To get this initial state, the incremental isotropic pressure was applied to an artificial packing of discs until the isotropic confining pressure $\sigma_0$ was attained. The constants used are listed in Table 1. The bars in Fig. 5 show the contact force vectors whose intensities are represented by the thicknesses. In the following, $\sigma_1$ and $\sigma_2$ denote the principal stresses in vertical and horizontal directions and are defined as the sums of pore pressure and effective stresses applied to grains; $\sigma_1'$ and $\sigma_2'$.

The cyclic loading was controlled by the increment of shearing stress $(\sigma_1-\sigma_2)/2$, while the mean stress $\sigma_0=(\sigma_1+\sigma_2)/2$ was kept constant under the undrained condition. The walls were controlled not to rotate and to move symmetrically with respect to the central axes in vertical and horizontal directions. The number of loading cycles was four and each cycle consisted of 40 steps.

Figure 6 shows the relationship between the shearing stress and the effective mean stress $\sigma_m'=(\sigma_1'+\sigma_2')/2$. The stress-strain relationship is given in Fig. 7. The

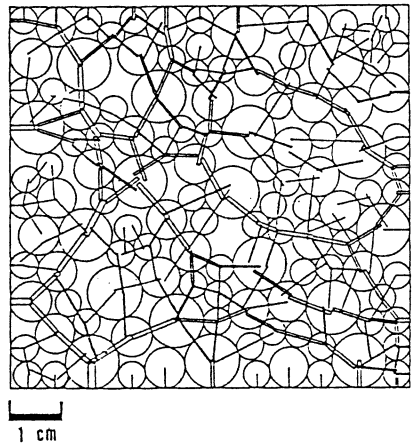


Fig. 5. Distribution of contact forces in the initial state.

Table 1. Constants used in the analysis (depth=1 cm).

| | |
|---|---|
| Diameter of disc | 6, 9, 12 mm |
| Initial void ratio | 0.26 |
| Weight of disc in water | $1.5 \times 10^3$ dyn/cm$^2$ |
| Stiffness $k_n$, $k_t$ | $1 \times 10^8$, $7 \times 10^7$ dyn/cm |
| Friction angle | 25° (between discs) |
| | 0° (between disc and wall) |
| Cohesion $c$ | 0 dyn |
| Bulk modulus of water | $1 \times 10^{10}$ dyn/cm$^2$ |
| Confining stress $\sigma_0$ | $1.5 \times 10^5$ dyn/cm |
| Increment of shearing stress | $\pm 2.5 \times 10^3$ dyn/cm |
| Amplitude of shearing stress | $\pm 2.5 \times 10^4$ dyn/cm |
| Modification factor | |
| $\alpha, \alpha', \beta, \beta'$ | 0.75, 0.5, 20, 20 |
| Accuracy $a$ | 100 dyn |

numbers attached in these figures represent the numbers of preceding loading steps. If the uneven changes in these diagrams are omitted, they are very similar to the results obtained by actual tests on sands. The first remarkable changes both in effective mean stress and in shearing strain correspond to the initiation of liquefaction, and they are observed during the third cycle. The last part of the loading path in Fig. 6 exhibits the so-called cyclic mobility. It is naturally observed from this part that the global friction angle of granular assembly is less than that of individual grains.

Figure 8 shows the distributions of contact forces at the end of loading step 109 and at the final state. The loading step 109 is the last step before the first remarkable change in the shearing deformation took place. As shown in Figs. 5 and 8, the intensities of contact forces decrease as the pore pressure increases. Most of the

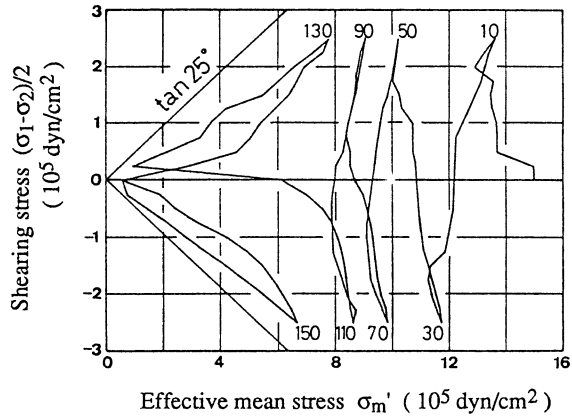


Fig. 6. Effective stress path.

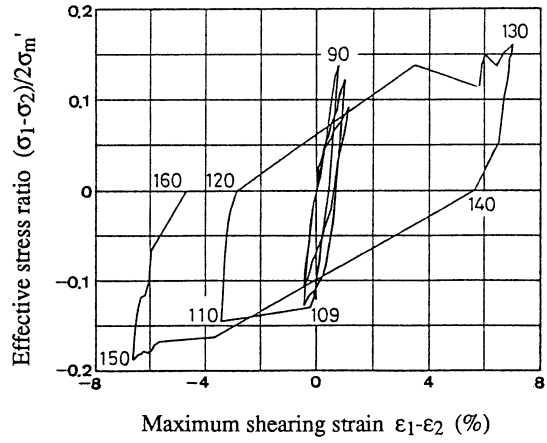


Fig. 7. Stress-strain relationship.

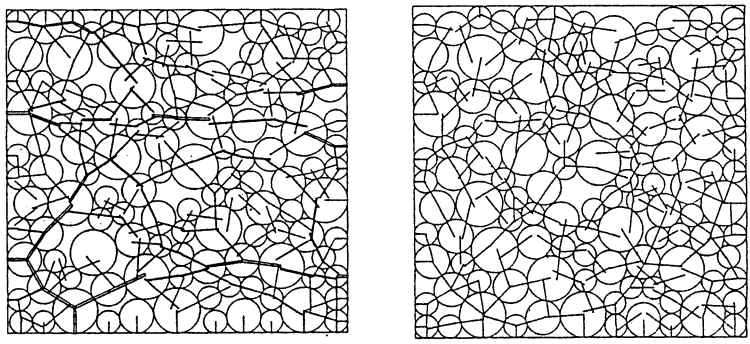

(a) (b)

Fig. 8. Distribution of contact forces. (a) The end of Step 109. (b) Final state.

grains have scarcely moved until the step 109, even though rather large pore pressure has developed. After this step, the grains change their locations in some extent with the remarkable change in shearing strain. However, as observed in these figures, the movements of grains do not follow the homogeneous deformation. In the following, the mechanical inhomogeneity in granular assemblies is discussed in terms of the dissipation energy.

Figure 9 shows the evolutions of total dissipation energy and total work. The amount of dissipation energy in this figure was obtained by subtracting the difference between elastic energies in current and initial states from the total work. The dissipation energy could be also calculated from Eq. 25, and the incremental values obtained by both methods agreed in most loading steps. However, there were some disagreement at several steps where the linear assumption in Eq. 25 failed. It is observed from this figure that the dissipation energy increases monotonously while the total work drops down slightly at the steps after the loading direction was reversed. By virtue of the relaxation of elastic energy stored in the initial state, the dissipation energy always exceeded the external work.

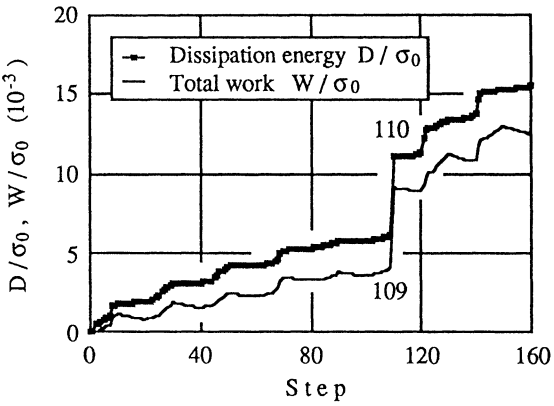


Fig. 9. Evolutions of dissipation energy and total work.

In Table 2, the incremental dissipation energies $\Delta D$ at the major steps are listed in order of the amount of dissipation. The largest dissipation took place in the loading step 110 during the third loading cycle. As stated above, the first remarkable shearing strain was observed in this step, but the incremental change in pore pressure is rather small as shown in Fig. 6. On the contrary, the drastic change in pore pressure took place in the loading step 121 whose incremental dissipation energy is ranked in the second. Thus, no correlation is observed between the pore pressure and the amount of dissipation itself. In the following, the distribution characteristics of the dissipation energy is discussed.

Figure 10 represents the distributions of dissipation energy for six major loading steps. In these figures, $P$ indicates the percentage of the dissipation energy at a single contact point for each loading step, and $N$ is the number of contact points

Table 2. Incremental dissipation energy at major steps.

| Ranking | Step | Cycle | $\Delta D/\sigma_0$ | $P_{max}$ |
|---|---|---|---|---|
| 1 | 110 | 3 | $2.739 \times 10^{-3}$ | 17.9% |
| 2 | 121 | 4 | .767 | 28.4 |
| 3 | 8 | 1 | .524 | 29.5 |
| 4 | 2 | 1 | .429 | 59.4 |
| 5 | 69 | 2 | .299 | 16.9 |
| 6 | 26 | 1 | .285 | 47.8 |
| 7 | 47 | 2 | .282 | 20.3 |
| 8 | 45 | 2 | .224 | 26.0 |
| 9 | 122 | 4 | .205 | 20.9 |
| 10 | 142 | 4 | .180 | 13.6 |
| 11 | 27 | 1 | .178 | 36.5 |
| 12 | 126 | 4 | .176 | 23.3 |
| 13 | 30 | 1 | .174 | 30.7 |
| 14 | 70 | 2 | .172 | 15.7 |
| 15 | 141 | 4 | .163 | 20.9 |
| 16 | 6 | 1 | .160 | 31.9 |
| 17 | 5 | 1 | .157 | 17.0 |
| 18 | 68 | 2 | .155 | 32.7 |
| 19 | 50 | 2 | .150 | 10.2 |
| 20 | 139 | 4 | .113 | 62.2 |

where the extent of dissipation energy exceeds $P$ percent. The maximum value of $P$ is separately listed in Table 2 as $P_{max}$.

The relationship between $P$ and $N$ for the loading step 2 is almost linear in log scales, which means that the distribution has the fractal nature, and it is noted that $P_{max}$ takes the value more than 50%. The granular assembly in such an earlier stage has not been prepared for the shearing deformation and the magnitudes of dissipation at contact points are scattering without the mean value, and the increment of pore pressure takes comparatively large value.

As the cyclic loading proceed to the intermediate stage represented by the steps 69 and 100, the granular assembly once becomes a "mature state". The pattern of distribution in such a state is smooth and the distribution has the tendency to become homogeneous with respect to the major contact points. It is noted that $P_{max}$ takes relatively small value, and that the increment of pore pressure is also comparatively small as observed in Fig. 6.

In the final stage represented by the loading step 121, the pore pressure changes drastically and the shape of distribution of dissipation energy has a characteristic pattern as shown in Fig. 10f and $P_{max}$ again takes rather large value. The rapid change in pore pressure is accompanied by the structural change in granular assembly and the distribution of dissipation energy during such a process is inhomogeneous. For drained tests, this process corresponds to the rapid volumetric change in granular assembly with unstable structures and the irreversible compaction takes place by virtue of the external confining pressure.

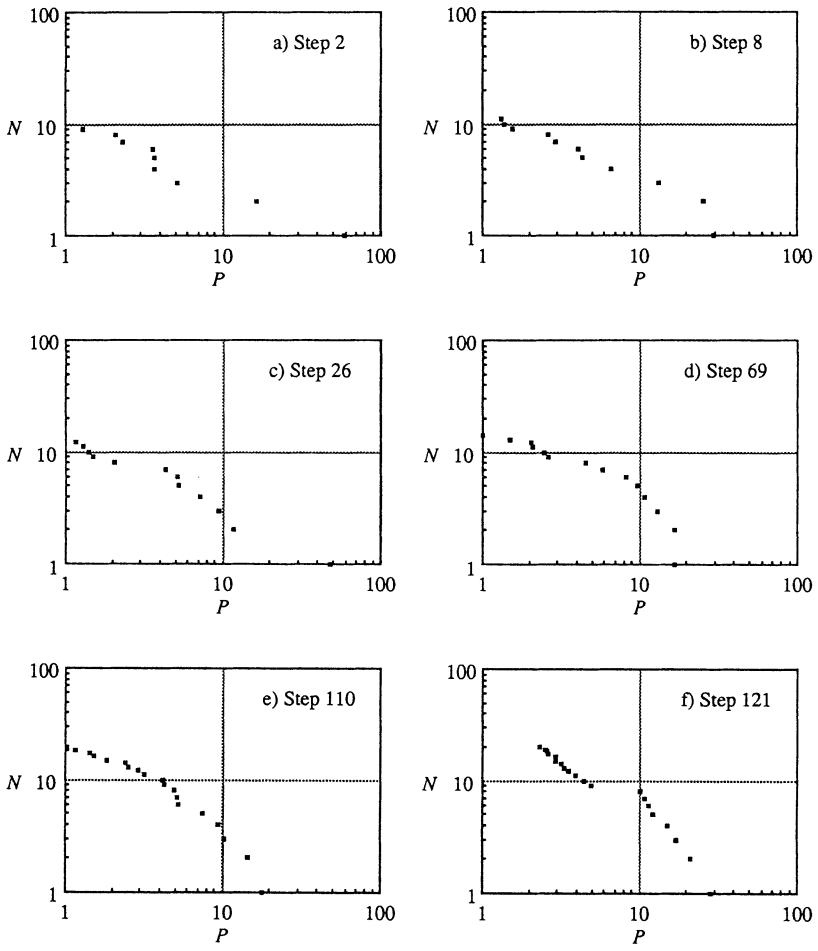


Fig. 10. Distribution of incremental dissipation energy.

## CONCLUDING REMARKS

The simulated results shown in this paper are qualitatively similar to the results obtained by the usual cyclic tests on real sands. The granular element method explained in the first part of this paper enables us to know not only the macroscopic behavior of granular materials but also the micromechanical informations such as the locations of grains, the distribution of contact forces or the distribution characteristics of dissipation energy. In this paper, the micromechanical process in the liquefaction phenomena was investigated through the detailed observation of dissipation energy.

It was found that the number of contact points which share the dissipation energy in each loading step is limited and, in several loading steps, there exists a contact point where the dissipation exceeds more than 50% of whole incremental

dissipation energy. There was a tendency that the distribution of dissipation energy is inhomogeneous when the large pore water pressure arises. The distribution characteristics of dissipation energy in the earlier stage had fractal nature. However, by the cyclic loading, the distribution pattern changed successively. It can be said that this is the process by which the granular assembly is mechanically adjusted to resist against the external action. The granular assembly once becomes a "mature state" where the mechanical behavior seems to be stable. However, there still exists a possibility to deform beyond this state and to get large pore water pressure as shown in the example.

To investigate further on liquefaction, many other tests should be done under different conditions such as different initial packings or different amplitudes of cyclic loading. However, the fundamental idea obtained in the example may be useful to introduce the rational constitutive equations for granular materials. The computer used for the analysis was a 32-bit engineering work station. The drawback of the granular element method may be that it requires long computational time. It sometimes requires many days for an entire numerical test. However, we can use it to get new informations on micromechanics of granular materials.

## REFERENCES

Cundall, P. A. and Strack, O. D. L. (1979): A discrete numerical model for granular assemblies. *Géotechnique*, **29**/1: 47–65.

Drescher, A. and de Josselin de Jong, G. (1972): Photoelastic verification of a mechanical model for the flow of a granular material. *J. Mech. Phys. Solids*, **20**: 337–351.

Kishino, Y. (1988): Disc model analysis of granular media. *Micromechanics of Granular Materials*. [ed. M. Satake and J. T. Jenkins. Amsterdam. Elsevier. 366.]: 143–152.

Satake, M. and Jenkins, J. T. / editors (1988): *Micromechanics of Granular Materials*. [Amsterdam. Elsevier. 366.]

## DISCUSSION

Q1. You showed us the distribution of contact forces between particles. Did you adopt a special method to represent the contact forces? (Takaki, R.)

A1. I am using usual method. The contact force vectors are represented by bars. The axis of a bar corresponds to the direction of contact force and the thickness is proportional to the intensity. The bar is drawn to intersect the contact point and it is common for two particles. The length, being equated to the sum of the radii of two particles, has no significant meanings.

Q2. How does the packing density change through the cyclic loading? (Brakenhoff, G. J.)

A2. The test was performed under the condition that the pore water can not escape. So, the volume of the granular assembly was almost constant. Instead of the volume, the pore water pressure developed and it led the granular assembly to the state of liquefaction. If the test was performed under the undrained condition, the volume change might be observed. The densification

in drained test corresponds to the increase of pore water pressure in undrained test.

Q3. Was the initial packing arranged so that the majority of force was transmitted through the large particles? (Nakagawa, M.)

A3. The initial arrangement was obtained through the isotropic stressing for an artificial packing which even did not fulfill the equilibrium conditions. The pattern of the distribution of contact forces was formed during the stressing. The similar pattern is also found in the photoelasticity tests on granular models.